Impurities bound to vacancies in insulators: Electronic relaxation and physical properties of the Cr^{3+}-V_M model center in KMF_3 (M = Mg, Zn)

P. García-Fernández,[1] A. Trueba,[1] B. García-Cueto,[1] J. A. Aramburu,[1] M. T. Barriuso,[2] and M. Moreno[1]

[1]*Departamento de Ciencias de la Tierra y Física de la Materia Condensada, Universidad de Cantabria, Avenida de los Castros s/n, 39005 Santander, Spain*

[2]*Departamento de Física Moderna, Universidad de Cantabria, Avenida de los Castros s/n, 39005 Santander, Spain*

This work is aimed at gaining a better insight into the influence of a close vacancy, V, on the properties of impurities in insulating materials. To achieve this goal the $Cr^{3+} - V_M$ model center formed in KMF_3 (M = Mg, Zn) fluoroperovskites has been explored in detail by means of *ab initio* calculations on clusters involving up to 87 ions. It is shown that the presence of the M^{2+} vacancy, V_M, induces a significant structural relaxation on the CrF_6^{3-} cubic complex which cannot be fully understood assuming that ions were rigid spheres that could not be polarized. Thus, although V_M forces all the ligands to move away, the $Cr^{3+} - F^-$ distance corresponding to the furthest ligand, F_{far}, is found to be slightly higher than that for the closer equatorial ions. This unexpected fact is shown to be due to the electronic relaxation also induced by V_M on the CrF_6^{3-} complex, causing a charge of $0.2e$ to be transferred from the closest ligand to V_M, F_{next}, mainly to F_{far}, and, to a lesser extent, to any equatorial ligand. This transfer of charge is mainly accomplished through orbitals lying in planes containing the C_4 axis. In spite of these changes due to the vacancy, the $^4A_{2g} \rightarrow {}^4T_{2g}$ optical transition is found to be weakly altered, a fact that concurs with available experimental data and whose origin is discussed. In contrast, electron paramagnetic resonance parameters such as gyromagnetic or superhyperfine tensors, which do depend on the electronic density around a point of the CrF_6^{3-} complex, are shown to be particularly sensitive to the electronic relaxation induced by V_M. In particular, the present study explains that the dominant component of the superhyperfine tensor for the F_{next} ligand is clearly higher than that for F_{far}, in agreement with experimental data. The relevance of the present results for understanding the electronic properties of other systems involving vacancies is also discussed. Some results on the $Cr^{3+} - Li^+$ center formed in $KMgF_3$ are also discussed for comparison.

I. INTRODUCTION

Vacancies play a relevant role in the physics of real crystalline compounds. Indeed, these defects are behind the diffusion and mass transport phenomena in crystals[1] while their motion under an applied electric field is the dominant mechanism responsible for electrical conductivity in a great deal of ionic solids.[2,3]

In an insulating material, the number of vacancies can be increased significantly by suitable doping. If in this process H^{c+} cations of the host lattice are substituted by I^{q+} impurity cations, where $q \neq c$, then the global charge compensation can lead to a huge increase of positive or negative vacancies with respect to those formed in the pure compound. The enhancement of vacancy concentration through doping increases the ionic conductivity of the material[2] and favors the formation of F and hole centers under X irradiation. This fact is used to build sensitive x-ray dosimeters.[4] When an H^{c+} cation of an insulating host lattice is replaced by an impurity ion I^{q+} ($q > c$), this process also gives rise to the formation of *complex centers* where the impurity, I, is bound to one positive vacancy, V, or more. If the impurity is a transition-metal cation not coupled to any other defect, then its unpaired electrons are usually *localized* in the IX_N unit formed with the nearest anions or ligands, X.[5] If the local symmetry of that IX_N unit embedded in the insulating lattice is octahedral, the addition of a vacancy near one of the ligands necessarily lowers the symmetry. The formation of this kind of I–V complex center formed in insulators was demonstrated early in the pioneering work by Watkins on Mn^{2+}-doped alkali chlorides by means of electron paramagnetic resonance (EPR) measurements.[6] Later on, several other works looked into such I–V complex centers by magnetic and optical techniques in cases when I is a transition-metal cation.[7–13] The importance of the impurity-vacancy defects has been stressed by several works, showing that they have a substantial impact on ferroelectric and piezoelectric properties of perovskite-type metal oxides, such as switching behavior, electrical aging, and polarization fatigue.[14,15] Along these lines, many studies have looked into the influence of the impurity-vacancy defects on the properties of manganites seeking to improve the magnetoresistance.[16]

Despite the relevance of complex I–V centers in insulating materials, a detailed knowledge of both their actual geometrical and electronic structure is still lacking. In general, the presence of vacancies bound to a transition-metal impurity in an insulating material is expected to induce not only changes of impurity-ligand distances but also a *rearrangement* of the electronic density. This modification on the electronic density is unfortunately very often unknown, although it is likely to play a key role for understanding the physicochemical properties of complex I–V centers. For this reason, a detailed knowledge of the electronic relaxation induced by a vacancy is a prerequisite in the search of reliable force fields for dealing with problems involving a huge number of atoms.[17] In spite of this fact, the interpretation of *available* EPR data of complex centers in insulating materials has often been based on empirical models related to a crystal-field description. In this kind of model, such as happens in the widely used superposition model,[10,13,18–20] the characteristics of ions (such
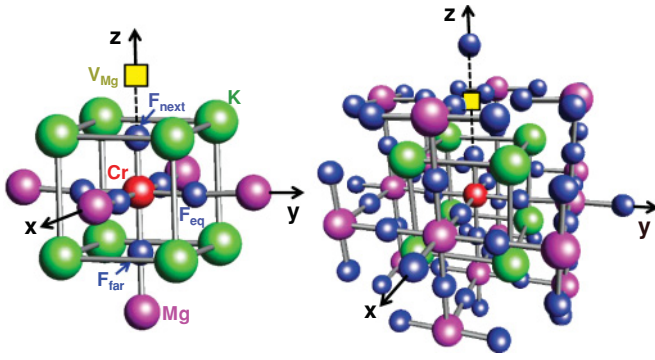
FIG. 1. (Color online) Clusters of 20 ions (left) and 86 ions used in the DFT calculations of the tetragonal $Cr^{3+} - V_{Mg}$ center in $KMgF_3$: Cr^{3+}. Notation used for the four fluorine ions in the equatorial plane, F_{eq}, and axial fluorines next, F_{next}, and far, F_{far}, from the vacancy is indicated on the left cluster.

as the total charge) are assumed not to change when they are transferred from a high-symmetry unit to another one with lower symmetry. An *ab initio* study carried out on both the FeF_6^{3-} (O_h symmetry) and the $C_{4v}FeF_5O^{4-}$ centers formed in KMF_3 fluorides ($M = Mg, Zn$) demonstrated that changes on the electronic density of F^- ions due to the presence of an O^{2-} ligand cannot be neglected at all.[5,21]

Seeking to improve our knowledge on complex *I–V* centers in insulating materials, we want to explore the *model* center $Cr^{3+} - V_M$ formed in cubic fluoroperovskites such as KMF_3 ($M = Mg, Zn$) doped with Cr^{3+}.[11,22–26] In that center, a close M^{2+} vacancy, V_M, is bound to the impurity, as shown in Fig. 1. To achieve this goal and gain a better insight into the ensemble of optical and EPR data on this center, *ab initio* calculations have been carried out on the tetragonal (C_{4v} symmetry) $Cr^{3+} - V_M$ center in $KMgF_3$. Aside from its relatively high symmetry, there are two main reasons to explore this center: (i) The vacancy bound to the Cr^{3+} ion comes from a divalent Mg^{2+} ion and thus its effects are expected to be bigger than if it replaces a monovalent ion such as K^+; (ii) there are optical and EPR data reported on this center that, to our knowledge, have not been well understood. Interestingly, partial information on superhyperfine (shf) tensors has been obtained by EPR for the $Cr^{3+} - V_M$ center formed in $KZnF_3$.[23]

Cr^{3+}-doped cubic AMF_3 fluoroperovskites ($A = K, Rb$; $M = Mg, Zn, Cd, \ldots$) have been extensively studied mainly for application as tunable solid-state lasers operating at room temperature.[27,28] In this kind of system, and also in layered perovskites such as K_2MgF_4 or K_2ZnF_4 doped with Cr^{3+}, different centers are usually *simultaneously* observed by means of EPR.[29,30] So, in lattices like $KMgF_3$, $KZnF_3$, or $RbCdF_3$ doped with Cr^{3+} aside from a pure cubic CrF_6^{3-} center,[22,23,31–33] there are other low-symmetry centers associated with the presence of a close A^+ vacancy ($A = K, Rb$), an M^{2+} vacancy ($M = Mg, Zn, Rb$), or an unwanted impurity.[7,22] It is also worth noting that for $KMgF_3$: Cr^{3+} codoped with Li^+ ions, another tetragonal $Cr^{3+} - Li^+$ center is formed just replacing Mg^{2+} by Li^+.[34] The observation by means of EPR of the cubic and $Cr^{3+} - V_M$ centers in fluoroperovskites means that the necessary charge compensation is *remote*.[22,23,29,30] A similar situation is encountered for the Jahn-Teller center $RhCl_6^{4-}$

formed in $NaCl:Rh^{2+}$ where the Na^+ vacancy is far apart from the Rh^{2+} impurity.[12]

It should be stressed here that although Cr^{3+}-doped $KMgF_3$, $KZnF_3$, and $RbCdF_3$ systems have also been explored optically, the position of the $^4A_{2g} \to {}^4T_{2g}$ transition of the cubic CrF_6^{3-} center, lying around $15\,000$ cm^{-1}, appears to be practically unmodified for centers with a vacancy.[11,25,26] In particular, the experiments carried out by Mortier *et al.* on $KMgF_3 : Cr^{3+}$ indicate that the region of the zero-phonon line for the $Cr^{3+} - V_M$ center would be redshifted by only ~150 cm^{-1} with respect to that corresponding to the cubic center.[11] Moreover, the expected splitting, Δ_T, on the $^4T_{2g}$ state for the tetragonal $Cr^{3+} - V_M$ center seems to be very small when compared to the ~1500 cm^{-1} bandwidth observed at low temperatures.[11] From the analysis of luminescence data obtained for the $Cr^{3+} - V_M$ center in $KZnF_3 : Cr^{3+}$, Vaills *et al.* suggested that such a splitting would be ~100 cm^{-1} (Ref. 24) and thus close to that measured for the ^2E state of the $Cr^{3+} - V_M$ center in MgO (93 cm^{-1}).[35] Nevertheless, if optical data seem to suggest that the presence of the vacancy produces only very small effects on the properties of the CrF_6^{3-} unit, this idea is no longer true when we look into EPR data. For instance, in the tetragonal $Cr^{3+} - V_M$ center formed in $KZnF_3$, EPR data at room temperature give $g_{||} = 1.975$ and $g_\perp = 1.978$ and thus a *clear anisotropy* is seen in the experimental g tensor.[23] Such anisotropy is indirectly related to the separation, Δ_T, between the $^4B_2$ and ^4E states in C_{4v} symmetry emerging from $^4T_{2g}$. In the *usual* framework of crystal-field theory, $g_{||}$ and $g_\perp$ are related, respectively, to the energies $\Delta(^4B_2)$ and $\Delta(^4E)$ of such states measured with respect to that of the ground state $^4A_2$,[36]

$$g_0 - g_{||} = 8\xi^*/3\Delta(^4B_2), \quad g_0 - g_\perp = 8\xi^*/3\Delta(^4E), \quad (1)$$

where the value of the *reduced* spin-orbit coefficient, ξ^*, which accounts for the experimental $g_0 - g$ value of the *cubic* CrF_6^{3-} center, is equal to 165 cm^{-1}.[11,23,31–33] Using this ξ^* value now in Eq. (1), together with the experimental $g_{||}$ and $g_\perp$ figures, it turns out that $\Delta_T \equiv \Delta(^4E) - \Delta(^4B_2)$ would be around 2000 cm^{-1} for the $Cr^{3+} - V_M$ center, a conclusion that is not supported at all by optical data. This significant discrepancy thus suggests that the differences in electronic density between $^4B_2$ and ^4E states could help to conciliate EPR and optical data of the $Cr^{3+} - V_M$ center.

Along these lines, relevant experimental data on the shf interaction of unpaired electrons with different ligands was also reported by Binois *et al.* on the tetragonal $Cr^{3+} - V_M$ center formed in $KZnF_3$.[23] Indeed, this kind of information is scarce in the case of centers involving one or more vacancies. From the analysis of EPR data, these authors conclude that the two ligands called F_{next} and F_{far} in Fig. 1 have a very different shf tensor. More precisely, they are able to determine the shf constant, $A_{||}$, when $\mathbf{H} \parallel OZ$ in Fig. 1 for both axial ligands. For one of them, $A_{||} = -23$ MHz, while for the other one, $A_{||} = -34$ MHz. Although Binois *et al.*[23] are not able to identify which of these values corresponds to F_{next}, this experimental result already stresses the existence of a significant departure from cubic symmetry.

Bearing in mind these facts, the present work is aimed first at gaining a better insight into the structural and electronic relaxation that takes place when comparing the tetragonal

$Cr^{3+} - V_M$ center with the cubic CrF_6^{3-} one. Moreover, in a second step this study explores in some detail the role played by the M^{2+} vacancy for modifying in a different way the optical and magnetic properties associated with the Cr^{3+} impurity.

This paper is arranged as follows. Details on the methods employed in the calculations are reported in Sec. II, while the results and the corresponding discussions are given in Secs. III–VII. Sec. III is devoted to studying the equilibrium geometry, starting with an analysis of both the $KMgF_3$ lattice and the cubic CrF_6^{3-} center to check the reliability of employed methods. Later on, the structural relaxation induced by the vacancy in the tetragonal $Cr^{3+} - V_M$ center is explored and compared to that for the $Cr^{3+} - Li^+$ center formed in $KMgF_3$. Sec. IV is focused on the changes of the electronic density induced by the vacancy, paying special attention to the different relaxation undergone by the five mainly d orbitals of chromium. The calculated optical spectra for both the cubic CrF_6^{3-} and tetragonal $Cr^{3+} - V_M$ centers are reported and discussed in Sec. V, while the correlation between optical excitations and the g tensor anisotropy is analyzed in Sec. VI, paying attention to the role played by the electronic relaxation and the interpretation of available shf data. Some final remarks are included in Sec. VII.

II. COMPUTATIONAL DETAILS

Ab initio calculations have been performed on tetragonal $Cr^{3+} - V_M$ and $Cr^{3+} - Li^+$ centers in $KMgF_3$, and also the cubic CrF_6^{3-} center, using the cluster approximation.[5,37] The use of finite clusters for describing the properties of these centers is consistent with the highly localized character of the unpaired electrons residing essentially in the CrF_6^{3-} complex region.[37] Geometry optimizations have been performed in the standard spin-restricted and nonrelativistic Kohn-Sham formalism of the density-functional theory (DFT) by means of the Amsterdam density-functional (ADF) code.[38] Calculations were performed on clusters centered at the chromium impurity, including up to 86/87 ions (Fig. 1). We have introduced in all calculations the electrostatic potential due to the rest of the $KMgF_3$ lattice simulated by means of a set of point charges. These charges (about 250) are located in lattice positions around the cluster, although the values of the charges themselves are fitted to reproduce the right potential inside the cluster due to the infinite lattice using an Evjen-Ewald scheme.[37]

The two clusters used for modeling the tetragonal $Cr^{3+} - V_M$ center are depicted in Fig. 1. In the 20-ion $CrF_6K_8Mg_5^{15+}$ cluster, we have optimized the positions of chromium impurity and the three *inequivalent* groups of ligands (four equatorial fluorines, F_{eq}, one axial F^- next to the Mg^{2+} vacancy, F_{next}, and another axial F^- ligand far from the vacancy, F_{far}) while the rest of the cluster ions were kept frozen at their ideal lattice positions. In the case of the 86-ion cluster $CrF_6K_8Mg_5F_{24}Mg_{12}F_6F_{24}^{14-}$, the positions of second (K^+) and third (Mg^{2+}) neighbors to the impurity have also been optimized under the constrictions of the tetragonal C_{4v} symmetry. As discussed below, the main results obtained with the two clusters are rather similar. Corresponding clusters for the tetragonal $Cr^{3+} - Li^+$ center have 21 and 87 atoms, including a Li^+ ion replacing an Mg^{2+} cation. For the sake

of completeness, the properties of the cubic CrF_6^{3-} center have also been explored by means of clusters involving up to 87 atoms.

To ensure the reliability of the present results, the calculations have been performed using four different exchange-correlation functionals: the Vosko-Wilk-Nusair functional[39] in the local-density approximation (LDA), Becke-Perdew (BP86),[40,41] and Perdew-Wang (PW91)[42] functionals in the generalized gradient approximation (GGA), and finally the PBE0 hybrid functional,[43,44] which is the hybrid form of the Perdew-Burke-Ernzerhof (PBE) GGA functional with 25% of Hartree-Fock exchange. We have verified that the results obtained with the four functionals are close. For example, the interatomic distances corresponding to the equilibrium geometries differ less than 1%.

As is well known, standard DFT calculations (using LDA, GGA, or hybrid functionals such as PBE0) usually lead to good results for equilibrium geometries and electronic structures of transition-metal complexes. However, larger deviations with respect to experimental findings are usually obtained in the computed values of optical transitions. For this reason, optical transitions in this work have been derived by means of the very accurate wave-function-based complete active space self-consistent-field method corrected by the second-order many-body perturbation theory (CASPT2) first-principles method, which includes most of the electron correlation energy and usually yields excellent results.[45–48] We have employed the MOLCAS 6.7 program suite[49] to undertake these calculations. The active space employed in the final calculations involved the five mainly $Cr(3d)$ orbitals and the mainly $Cr(4s)$ one, containing a total of three electrons. Due to the increased computational cost of CASPT2 calculations with respect to DFT ones, the cluster size had to be reduced. Most calculations have been carried out in a CrF_6^{3-} complex surrounded by *ab initio* model potentials (AIMP's), which simulate very accurately the short-range interactions with the rest of the lattice,[50] to form a complex of 21 ions and point charges to simulate the field of the rest of the lattice. We checked that the results were converged with cluster size by performing some test calculations on a 21-ion cluster $CrF_6K_8Mg_6^{17+}$ where all ions were treated quantum mechanically. The electronic transitions reported in this work have all been calculated using a large all-electron basis set.[51]

III. EQUILIBRIUM GEOMETRY

A. Pure $KMgF_3$ lattice

As a first step, we have carried out a test on the two clusters chosen to model all studied centers in $KMgF_3 : Cr^{3+}$ and also on the three exchange-correlation functionals used in the DFT calculations. The results are shown in Table I. In the case of the 21-ion $MgF_6K_8Mg_6^{16+}$ cluster simulating the host lattice, we have only optimized the position of F^- ligands. The obtained values of the distance, R_0, between the central Mg^{2+} ion and the F^- ligands for the three considered functionals are found to be *only less than* 1.2% higher than the experimental value measured by x-ray diffraction, $R_0 = 198.7$ pm.[52] In the case of the 87-ion $MgF_6K_8Mg_6F_{24}Mg_{12}F_6F_{24}^{13-}$ cluster, we have also optimized the positions of two layers of K^+ and Mg^{2+} ions.

TABLE I. Values of the $Mg^{2+} - F^-$ distance (in pm units) obtained in the geometry optimizations performed for the pure $KMgF_3$ lattice using clusters of two sizes and three different exchange-correlation functionals, LDA, GGA-BP86, and GGA-PW91. In the 86-ion cluster, the positions of the second (K) and third (Mg) neighbors have also been optimized. The experimental Mg-F distance is $R_0 = 198.7$ pm.[47]

Cluster	LDA	GGA-BP86	GGA-PW91
21 ions	199.9	201.1	200.8
87 ions	198.6	198.7	198.6

In this case, the calculated R_0 values for the three considered functionals practically coincide with the experimental figure.

B. Octahedral $KMgF_3 : Cr^{3+}$ center

Once we verified that the clusters used in this study give reasonable results for the $KMgF_3$ pure lattice, we calculated the structural relaxation on the local geometry induced by the $Mg^{2+} \rightarrow Cr^{3+}$ substitution in the cubic $KMgF_3 : Cr^{3+}$ center. Results given here correspond to the $^4A_{2g}(t_{2g}^3)$ ground state of the CrF_6^{3-} unit. When the $CrF_6K_8Mg_6^{17+}$ cluster is used, the value obtained with the LDA functional for the $Cr^{3+} - F^-$ distance is found to be $R = 190.4$ pm, thus implying an inward relaxation of 9.5 pm. The same R value within 1% is obtained using the GGA-BP86, GGA-PW91, and hybrid PBE0 functionals. Results obtained using the $CrF_6K_8Mg_6F_{24}Mg_{12}F_6F_{24}^{12-}$ cluster are given in Table II and compared to the values previously reported by López-Moraza *et al.*[53] using CASSCF calculations on a seven-atom CrF_6^{3-} complex embedded in frozen model potentials. It should be pointed out that values obtained with the two GGA functionals differ less than 1.5 pm with respect to the corresponding LDA values given in Table II.

It can be noted that our results on the 87-ion cluster lead to an *inward* relaxation of F^- ligands equal to 7.5 pm, which is thus close to previous findings for the CrF_6^{3-} center in $KMgF_3$ (Ref. 54) and K_2MgF_4 lattices[37] and consistent with the smaller ionic radius of Cr^{3+} when compared to that of Mg^{2+}. As a salient feature second-neighbor K^+ ions and third-neighbor Mg^{2+} ions are found to relax *outward*. A similar trend emerges from the previous work by López-Moraza *et al.*,[53] although the reported relaxation for K^+ ions appears to be overestimated as it is bigger than that for the F^- ions of the first shell. The *outward* relaxation of positive K^+ and

TABLE II. Variation, $\Delta R(F)$, of the metal-ligand distance due to the $Mg^{2+} \rightarrow Cr^{3+}$ substitution in the cubic CrF_6^{3-} center formed in $KMgF_3$ derived from the present DFT-LDA calculations using a $CrF_6K_8Mg_6F_{24}Mg_{12}F_6F_{24}^{12-}$ cluster. Outward relaxations undergone by the closest K^+, $\Delta R(K)$, and Mg^{2+}, $\Delta R(Mg)$, ions are also given. The results are compared to those previously reported by López-Moraza *et al.*[48] All values are given in pm units.

	$\Delta R(F)$	$\Delta R(K)$	$\Delta R(Mg)$
This work	−7.5	5.4	1.7
López-Moraza *et al.*	−6.5	11.8	2.4

Mg^{2+} ions is qualitatively consistent with the extra positive charge introduced by the $Mg^{2+} \rightarrow Cr^{3+}$ substitution.[37] A quite similar situation has been discussed for $NaCl : Rh^{2+}$.[55,56] It should be noticed that in cases in which the impurity has a higher nominal charge than the host lattice cation, the different relaxation undergone by the first two shells of ions means that centers like CrF_6^{3-} in $KMgF_3$ or K_2MgF_4 or $RhCl_6^{4-}$ in NaCl are to a good extent elastically decoupled from the rest of the lattice.[5]

C. Tetragonal $Cr^{3+} - V_M$ and $Cr^{3+} - Li^+$ centers in $KMgF_3$

In a further step, we explored how the presence of a close Mg^{2+} vacancy along the [001] direction modifies the position of all ions involved in the CrF_6^{3-} unit and also that of other close ions of the $KMgF_3$ lattice. Results of DFT calculations for the tetragonal $Cr^{3+} - V_M$ center using clusters of 20 and 86 ions are gathered in Table III. As the results derived by means of LDA, GGA-BP86, GGA-PW91, and PBE0 functionals are essentially the same, we have included in Table III only those obtained with the LDA functional. For the sake of completeness, results corresponding to the structural relaxation in the $Cr^{3+} - Li^+$ center in $KMgF_3$ are also gathered in Table III.

The results of Table III for the $Cr^{3+} - V_M$ center in $KMgF_3$ obtained with clusters of 20 and 86 ions show a similar trend. Taking as a guide the results derived with the biggest cluster, the presence of the Mg^{2+} vacancy moves away all ions of the CrF_6^{3-} unit. Furthermore, as a result of the Mg^{2+} vacancy, not all three different $Cr^{3+} - F^-$ distances are now equal. In particular, the distance, $R(F_{next})$, between Cr^{3+} and the ligand termed F_{next} in Fig. 1 is reduced by 13 pm on passing from the cubic CrF_6^{3-} unit to the $Cr^{3+} - V_M$ center. With regard to the four equatorial ligands lying farther from the vacancy, their distance to the Cr^{3+} impurity is found to increase only about 1 pm with respect to the value 191.2 pm corresponding to the cubic CrF_6^{3-} unit. It is worth noting now that although the ligand ion denoted F_{far} in Fig. 1 is the farthest one from the vacancy, its distance to Cr^{3+} is found to increase by 3.3 pm, that is, 2.3 pm more that the equatorial ligands. This surprising fact can be understood taking into account the variations of electronic charge on ligands due to the vacancy, an issue analyzed in the next section.

The results conveyed in Table III for the $Cr^{3+} - V_M$ center point out that under the influence of the vacancy, the Cr^{3+} ion moves away from it. This result is seemingly surprising as the Mg^{2+} vacancy behaves as a negative charge, thus attracting the Cr^{3+} ion. This counterintuitive shift can be understood as a result of the strong bonding between Cr^{3+} and the six F^- ligands. As all F^- anions move away from the vacancy (Table III), they drag the Cr^{3+} cation. To support this view, we performed a calculation optimizing only the position of the Cr^{3+} ion, keeping the ligands in the positions of the cubic center. We found that in this case, the chromium ion moves 13.2 pm *toward* the vacancy.

Although the active electrons in the complex $Cr^{3+} - V_M$ center are also found to reside essentially on the impurity and six ligands it should also be remarked that the four closest K^+ ions to the vacancy also experience a significant structural relaxation. In fact, they are found to move 23.6 pm toward

TABLE III. Calculated Cartesian coordinates (in pm units) of the central Cr^{3+} ion and F^- ligands obtained in the geometry optimizations performed for the tetragonal $Cr^{3+} - V_{Mg}$ and $Cr^{3+} - Li^+$ centers in $KMgF_3$ using clusters of two sizes. The Mg^{2+} vacancy or the Li^+ ion are both placed in the [001] direction. The origin of the coordinates corresponds to the position of an Mg^{2+} ion in the perfect lattice. In both centers, the substitutional Cr^{3+} ion is shifted outward from that position. In the 86/87-ion clusters, the positions of the second (K) and third (Mg) neighbors have also been optimized. Moreover, in the 87-ion cluster modelling the $Cr^{3+} - Li^+$ center, the coordinates of the Li^+ ion were also varied. Metal-ligand distances, R, are also given in italic letters.

Center	Cluster	Cr	F_{eq}	F_{next}	F_{far}	Li
$Cr^{3+} - V_{Mg}$	20 ions	(0,0, −7.4)	(193.5,0, −16.7)	(0,0,166.3)	(0,0, −206.0)	
			193.7	*173.7*	*198.6*	
	86 ions	(0,0, −8.6)	(192.2,0, −13.5)	(0,0,169.7)	(0,0, −203.1)	
			192.3	*178.3*	*194.5*	
$Cr^{3+} - Li^+$	21 ions	(0,0, −6.5)	(193.1,0, −10.3)	(0,0,172.8)	(0,0, −200.9)	
			193.1	*179.3*	*194.4*	
	87 ions	(0,0, −0.8)	(192.5,0, −5.0)	(0,0,181.4)	(0,0, −192.7)	(0,0,419.5)
			192.8	*182.2*	*191.9*	

the Mg^{2+} vacancy while the next shell of K^+ ions moves only 4.2 pm. In contrast, the nearest Mg^{2+} ions are only moved 2.1 pm by the presence of the vacancy.

Despite the fact that the presence of the Mg^{2+} vacancy induces a tetragonal C_{4v} distortion on the CrF_6^{3-} unit, it is worth noting that the *average* $Cr^{3+} - F^-$ distance obtained in the calculation performed for the 86-ion cluster coincides within 1 pm with the calculated equilibrium distance for the cubic CrF_6^{3-} unit. This result already suggests that the 10 Dq splitting parameter for the $Cr^{3+} - V_M$ center is likely to be not very different from that for the CrF_6^{3-} unit. Nevertheless, the significant distortion induced by the vacancy could give rise to a measurable splitting in the first excited state $^4T_{2g}$. These matters are analyzed in detail in Sec. III E.

In the case of the tetragonal $Cr^{3+} - Li^+$ center (Table III), the replacement of the divalent Mg^{2+} ion by the monovalent Li^+ ion leads, as expected, to a smaller structural relaxation of all ligand ions than that found for the $Cr^{3+} - V_M$ center. For instance, the $Mg^{2+} \rightarrow Li^+$ substitution leads to a 4.7% reduction of $R(F_{next})$ with respect to the value 191.2 pm found for the cubic CrF_6^{3-} unit, while such a reduction is equal to 6.8% in the case of the $Cr^{3+} - V_M$ center. Despite the different structural relaxation in both centers, the *average* $Cr^{3+} - F^-$ distance in the $Cr^{3+} - Li^+$ center is also close to that calculated for the cubic CrF_6^{3-} unit. As the Li^+ ion substituting Mg^{2+} behaves like a charge $-e$, it undergoes, as shown in Table III, an outward displacement about 20 pm from its initial position. It is noteworthy that in the $Cr^{3+} - Li^+$ center, the $Cr^{3+} - F_{far}$ distance is slightly smaller than the $Cr^{3+} - F_{eq}$ one, while in the $Cr^{3+} - V_M$ center, the reverse is true. In the next section, we will analyze the relationship between this result and the bigger electronic relaxation in the $Cr^{3+} - V_M$ center where the vacancy of a divalent cation is involved.

In a recent study carried out on both $Cr^{3+} - V_M$ and $Cr^{3+} - Li^+$ centers in $KMgF_3$ by means of the empirical superposition model, it was concluded that the equilibrium geometry for both centers is essentially the same.[57] In particular, a value $R(F_{next}) = 185$ pm is found for the two centers. This conclusion is certainly hard to believe bearing in mind that the removal of Mg^{2+} and its replacement by Li^+ does not convey the same variation of charge. This idea is in agreement with the results of Table III showing that $R(F_{next})$ is 4 pm smaller for the $Cr^{3+} - V_M$ center when compared to the $Cr^{3+} - Li^+$ one. On the other hand, in the study based on the superposition model, it is assumed that $R(F_{far}) = R(F_{next})$.[57] This statement is, however, not supported by the results gathered in Table III for the $Cr^{3+} - V_M$ center.

IV. ELECTRONIC RELAXATION INDUCED BY THE VACANCY IN THE $Cr^{3+} - V_M$ CENTER

A key point in the present study is to look into the changes on the electronic density of a CrF_6^{3-} unit due to the presence of a close Mg^{2+} vacancy. To properly analyze all of the changes that happen on passing from the cubic CrF_6^{3-} center to the $Cr^{3+} - V_M$ one, such a transition is explored using five steps: (a) The departure point is the cubic CrF_6^{3-} center in $KMgF_3$ at the corresponding equilibrium geometry. (b) The $Cr^{3+} - V_M$ center is considered but *keeping* the equilibrium geometry of the cubic CrF_6^{3-} center. (c) The F_{next} ion closest to the vacancy (Fig. 1) is allowed to relax at the final equilibrium position of the $Cr^{3+} - V_M$ center. (d) Now the F_{far} ligand (Fig. 1) is also allowed to relax at the equilibrium position of the $Cr^{3+} - V_M$ center. (e) Finally, the $Cr^{3+} - V_M$ center at the right equilibrium geometry is considered.

A. Influence of electronic relaxation on Mulliken charges

Seeking to clear out the transfer of electronic charge, we have calculated the Mulliken charges for Cr^{3+} and the six ligand ions for every step. Results are gathered in Table IV. It can be observed in this table that the more drastic changes are produced on passing from step a to b, where the vacancy is introduced but the geometry is kept frozen. As shown in Table IV, smaller variations on the Mulliken charges are produced in the other steps. It should be noticed that in the $a \rightarrow b$ transition, an important decrement of the electronic charge associated with the F_{next} ligand takes place going from $-0.65e$ to $-0.39e$. In contrast, on passing from step b to the last step e, there is only a small increase of the charge on the F_{next} ligand equal to $0.06e$. As shown in Table IV, the electronic charge lost by F_{next} in the whole process is moved to F_{far} and F_{eq} ligands and the central cation. Moreover, we have verified

TABLE IV. Effect of the V_{Mg} vacancy on the Mulliken charge distribution (electron units) of Cr impurity and F ligands, calculated on 21/20-atom clusters simulating the cubic CrF_6^{3-} and tetragonal $Cr^{3+} - V_{Mg}$ centers. Total effect is divided in five steps (rows) corresponding to a, equilibrium geometry of the cubic Cr^{3+} center; b, introducing the V_M vacancy but maintaining the geometry; c, same as b but placing the F_{next} ligand at the final position given in Table III; d, same as c but placing the F_{far} ligand at the final position; e, equilibrium geometry of the $Cr^{3+} - V_{Mg}$ center.

Step	Cr				F_{eq}			F_{next}			F_{far}		
	Total	s	p	d	Total	s	p	Total	s	p	Total	s	p
a	+1.52	0.09	0.22	4.16	−0.65	2.02	5.62	−0.65	2.02	5.62	−0.65	2.02	5.62
b	+1.53	0.08	0.21	4.16	−0.67	2.02	5.64	−0.39	2.04	5.33	−0.68	2.02	5.66
c	+1.54	0.09	0.17	4.19	−0.67	2.02	5.64	−0.47	2.08	5.36	−0.68	2.02	5.66
d	+1.52	0.09	0.18	4.20	−0.67	2.02	5.64	−0.46	2.08	5.36	−0.68	2.01	5.67
e	+1.50	0.09	0.21	4.19	−0.66	2.01	5.64	−0.45	2.06	5.37	−0.68	2.01	5.65

that a total electronic charge of $0.1e$ is transferred to near K^+ and Mg^{2+} ions.

The results gathered in Table IV already point out that the *main* changes in electronic density appear when the vacancy is taken into consideration, but ligands are kept at the equilibrium positions corresponding to the cubic CrF_6^{3-} center. A similar conclusion is reached in the analysis of the transferred spin density on ligands shown in Sec. IV D.

It is worth noting now that in the whole process, the electronic charge of an F_{eq} ligand is found to increase only by $0.01e$ while the corresponding increase undergone by F_{far}, which is the *farthest* ligand from the vacancy, is three times bigger. These results help us to understand why $R(F_{far}) > R(F_{eq})$ for the $Cr^{3+} - V_M$ center. At the same time, they underline that an understanding of structural relaxation induced by the vacancy requires one to look into the effects that such a defect has on the electronic density.

B. Picture of the electronic relaxation through the deformation density

Due to the relevance of electronic relaxation, we have tried to visualize in more detail the changes of electronic density on a CrF_6^{3-} unit induced by the presence of a neighbor Mg^{2+} vacancy. According to the results of the preceding section, we have explored the changes of electronic density taking place in the $a \rightarrow b$ step using a 21/20-ion cluster. Let us designate by ρ(cubic) and ρ(tetragonal) the calculated electronic density for the cubic CrF_6^{3-} center and the $Cr^{3+} - V_M$ center frozen at the equilibrium geometry of the first species. As the removal of an Mg^{2+} ion modifies the total number of electrons in the cluster, we have then compared ρ(cubic) with ρ(tetragonal) + $\rho(Mg^{2+})$, where $\rho(Mg^{2+})$ corresponds to a free Mg^{2+} ion. Due to the ionic character of the bonding between Mg^{2+} and close fluorine ions, the inclusion of $\rho(Mg^{2+})$ should not obscure the main changes of electronic density on Cr^{3+} and six ligands. We have portrayed in Fig. 2 the changes undergone by the deformation density, $\Delta\rho(a \rightarrow b)$, in the $a \rightarrow b$ transition, where $\Delta\rho(a \rightarrow b)$ is simply given by

$$\Delta\rho(a \rightarrow b) = [\rho(\text{tetragonal}) + \rho(Mg^{2+}) - \rho(\text{cubic})]. \quad (2)$$

Figure 2 clearly shows that there is a significant rearrangement of the electronic density, particularly along the C_4 axis joining the vacancy, the chromium ion, and the two F_{next} and

F_{far} ligands. As depicted in Fig. 2, the presence of the Mg^{2+} vacancy forces a decrement of the electronic charge in the neighborhood of the F_{next} ligand while it increases in the region lying farther from the vacancy. This relevant modification of the electronic density around F_{next} and F_{far} ligands, consistent with the results collected in Table IV, indicates that their characteristics are certainly modified on passing from the cubic to the $Cr^{3+} - V_M$ center.

C. Changes induced on mainly 3d orbitals

In the case of the cubic CrF_6^{3-} center, the g factor is determined by the admixture of the $^4A_{2g}(t_{2g}^3)$ ground state with the excited $^4A_{2g}(t_{2g}^2 e_g^1)$.[36] While in the cubic center the
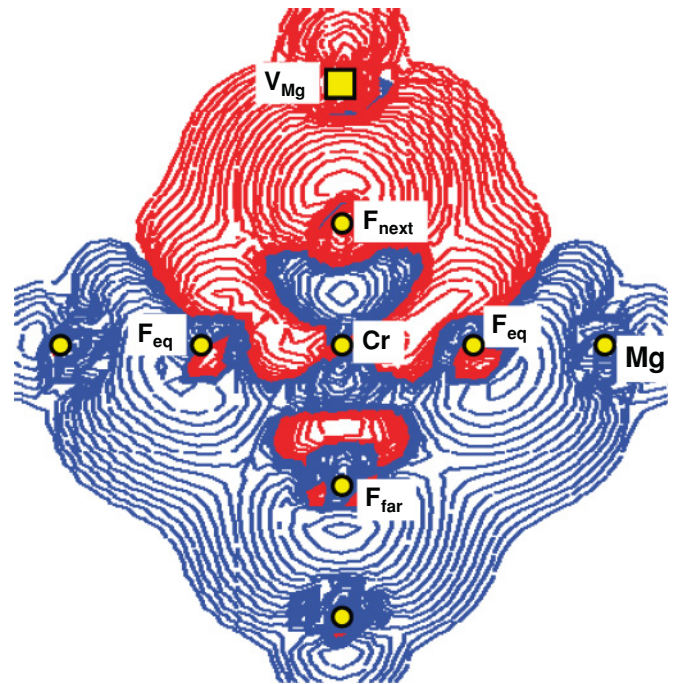
FIG. 2. (Color online) Plot of the deformation density, $\Delta\rho(a \rightarrow b)$, induced by the V_M vacancy on the cubic $CrF_6K_8Mg_6^{15+}$ cluster at frozen geometry (step $a \rightarrow b$). If the vacancy is located in the [001] direction, $\Delta\rho(a \rightarrow b)$ is depicted in the (100) plane containing F_{next}, F_{far}, and two F_{eq} ligands. Red and blue lines correspond to areas of decreased and increased density, respectively.

TABLE V. Values of the $[N(i)]^2$ quantity (in %) derived for the five antibonding orbitals through the present calculations. Results obtained for both cubic CrF_6^{3-} and tetragonal $Cr^{3+} - V_M$ centers are reported.

Center	$b_2(xy)$	$e(xz,yz)$	$b_2(x^2 - y^2)$	$a_1(3z^2 - r^2)$
cubic CrF_6^{3-}	87	87	80	80
$Cr^{3+} - V_M$	88.5	83	81	72

antibonding $x^2 - y^2$ and xy orbitals are strictly equivalent to $3z^2 - r^2$ and xz,yz, respectively, this is no longer true when we move to the $Cr^{3+} - V_M$ center. Let us consider an antibonding orbital of the CrF_6^{3-} complex briefly described by

$$|\phi(i)\rangle = N(i)|d_i\rangle - \lambda(i)|\chi_i^L\rangle \qquad (3)$$
$$(i = xy, xz, yz, x^2 - y^2, 3z^2 - r^2).$$

Here $|d_i\rangle$ means a d-wave function while $|\chi_i^L\rangle$ stands for a suitable linear combination involving valence orbitals of six ligands. Seeking to gain a general view on the effect of the vacancy upon *all* antibonding orbitals, we have calculated the $N^2(i)$ quantity for the $(xy)^{3/5}(xz)^{3/5}(yz)^{3/5}(x^2 - y^2)^{3/5}(3z^2 - r^2)^{3/5}$ configuration with fractional occupation where all orbitals are equally populated. The value of $N^2(i)$, reflecting the amount of electronic charge on chromium for the corresponding antibonding orbital, has been calculated for both the cubic and the $Cr^{3+} - V_M$ centers in $KMgF_3$. The results shown in Table V for the $Cr^{3+} - V_M$ center indicate that the charge on chromium is smaller by 9% for an $a_1(3z^2 - r^2)$ orbital pointing toward the vacancy than in the case of the other σ orbital, $b_1(x^2 - y^2)$, lying in the perpendicular plane to the Cr^{3+}-vacancy axis. A similar situation holds when comparing the $e(xz,yz)$ orbitals with the $b_2(xy)$ orbitals, which is placed in the same plane as $b_1(x^2 - y^2)$. Nevertheless, in this case where π orbitals are involved, the difference amounts only to 6%. The importance of the differences between $N^2(x^2 - y^2)$ and $N^2(3z^2 - r^2)$ for a proper understanding of the experimental $g_0 - g_\parallel$ value for the $Cr^{3+} - V_M$ center is stressed in Sec. VI A.

D. Spin density transferred on ligands in the cubic and $Cr^{3+} - V_M$ centers

If we have a transition-metal impurity, I, placed in a fluoride, the unpaired electrons are usually localized in the IF_N unit. Such a unit can be either isolated or coupled to a close defect, as happens in the case of the $Cr^{3+} - V_M$ center. In any half-filled antibonding orbital of the IF_N unit, the unpaired electrons spend some time on $2p\sigma$, $2p\pi$, or $2s$ levels of a given F^- ligand, as indicated in Eq. (2). This transfer is usually described by the f_σ, f_π, and f_s quantities.[36,58] As in the ground state, $^4A_{2g}(t_{2g}^3)$, of the octahedral CrF_6^{3-} unit, there are not unpaired electrons displaying σ bonding, therefore $f_\sigma = f_s = 0$ while $f_\pi = [\lambda(xy)]^2/4$ and $\lambda(xy)$ is defined in Eq. (3). Thus f_π just means the fraction of unpaired spin transferred to a *single* ligand orbital. It should be noted now that when a vacancy is present along the OZ axis, the two $p\pi$ orbitals of equatorial ligands are no longer equivalent. In such a case, we shall call $f_{\pi\parallel}$ and $f_{\pi\perp}$ the quantities associated with

TABLE VI. Calculated values (in %) of the $f_s, f_\sigma, f_{\pi\parallel}$, and $f_{\pi\perp}$ parameters of spin density transferred on, respectively, $2s$, $2p_\sigma, 2p_{\pi\parallel}, and 2p_{\pi\perp}$ orbitals of F_{eq}, F_{next}, and F_{far} ligands in the $Cr^{3+} - V_{Mg}$ center, for the five steps previously described. Calculations were performed for the ground state of 20/21-atom clusters.

| Step | F_{eq} | | | | F_{next} | F_{far} |
	f_s	f_σ	$f_{\pi\parallel}$	$f_{\pi\perp}$	f_π	f_π
a			4.56	4.56	4.56	4.56
b	0.24	0.05	4.24	3.37	10.53	3.50
c	0.51	0.09	4.03	2.80	12.84	3.41
d	0.74	0.11	4.05	3.00	12.68	2.56
e	0.29	0.11	4.12	3.28	9.61	3.29

the $p\pi$ orbitals parallel or perpendicular to the principal C_4 axis.

A main goal of the present analysis is to study how f_π is modified on going from an octahedral CrF_6^{3-} center to the $Cr^{3+} - V_M$ center. Calculated values of f_π for the six ligands of the two centers in $KMgF_3$ are displayed in Table VI. Aside from giving the values determined for the final equilibrium geometry of the $Cr^{3+} - V_M$ center, results corresponding to the intermediate steps previously described at the beginning of Sec. IV are also enclosed in Table VI. Similarly to what is found in previous sections, it can be noted that the more drastic changes are produced on passing from step a to b, where the vacancy is introduced but the geometry is kept frozen. From the present calculations, it is found for the F_{next} ligand that while $f_\pi = 4.6\%$ for the octahedral CrF_6^{3-} center, such a quantity increases until $f_\pi = 9.6\%$ for the $Cr^{3+} - V_M$ center at the corresponding equilibrium geometry. At the same time, the results in Table VI give $f_\pi = 3.3\%$ for the F_{far} ligand of the $Cr^{3+} - V_M$ center, which means a reduction with respect to the values for the octahedral CrF_6^{3-} unit. A smaller reduction is also found for f_π corresponding to the four equatorial ligands.

It is worth noting that the trends shown in Table VI are in qualitative agreement with those displayed by the Mulliken charges on passing from the octahedral CrF_6^{3-} unit to the $Cr^{3+} - V_M$ center (Table IV). In fact, if in a given antibonding level the presence of the vacancy increases the probability of finding the electron in the $2p$ orbital of the F_{next} ligand, the opposite happens for the counterpart bonding orbital. As the latter orbital is fully occupied while the antibonding is only partially occupied, this implies a reduction of the *total* electronic charge on the F_{next} ligand such as is reported in Table IV. The transfer of electronic charge induced by internal electric fields has recently been explored for $LiBaF_3 : Mn^{2+}$.[59]

E. Electronic levels in the $Cr^{3+} - V_M$ center

In this section, the electronic levels of the cubic CrF_6^{3-} and tetragonal $Cr^{3+} - V_M$ centers in $KMgF_3$, calculated at the corresponding equilibrium geometries, are compared. The main results obtained using DFT in 20/21-ion clusters are portrayed in Fig. 3. If we consider the cubic CrF_6^{3-} center,
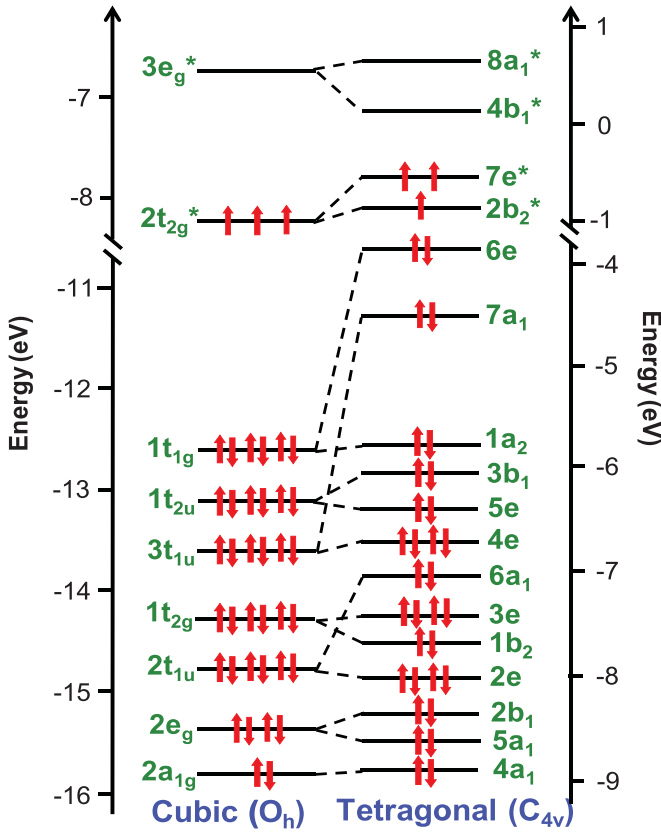
FIG. 3. (Color online) Diagram showing the variation of the molecular orbitals of the cubic CrF_6^{3-} center by introducing the V_M vacancy at frozen geometry (step $a \to b$). Results correspond to calculations on 21/20-ion clusters. Note the shift of the energy scale used for both centers.

the 18 molecular orbitals termed $2a_{1g}, 2e_g, 2t_{1u}, 1t_{2g}, 3t_{1u}, 1t_{2u},$ and $1t_{1g}$ are mainly built from the $2p$ wave functions of six ligands. In contrast, $2t_{2g}$ (which is semioccupied) and $2e_g$ are antibonding levels mainly made from $3d$-wave functions of chromium. Looking at Fig. 3, it can be noted that when the vacancy is introduced, it raises the energy of all orbitals, though not by the same amount. So, the two levels $7a_1$ and $6e$ in the C_{4v} center are lying well above the rest of the charge-transfer levels. Such levels are just those built mainly from $2p$ orbitals of the F_{next} ligand.

According to the C_{4v} symmetry of the $Cr^{3+} - V_M$ center, there is a splitting, δ_e, between the antibonding $8a_1(\sim 3z^2 - r^2)$ and $4b_1(\sim x^2 - y^2)$ orbitals coming from e_g in O_h symmetry. Similarly, there is also a smaller splitting, δ_t, between $7e(\sim xz, yz)$ and $2b_2(\sim xy)$ orbitals, which have a π character. For the sake of clarity, we have calculated the values of δ_e and δ_t at the equilibrium geometry of the $Cr^{3+} - V_M$ center and also for the other four steps previously described, and the results are gathered in Table VII. It can be noticed that the inclusion of the vacancy keeping the equilibrium geometry of the cubic center (step b) already gives rise to 60% and 45% of the *final* δ_t and δ_e splittings, respectively. Moreover, if only the ligand F_{next} is allowed to reach its equilibrium position, the calculated δ_t and δ_e values practically reproduce the final quantities.

TABLE VII. Calculated values of δ_t and δ_e orbital splittings (in eV) for the five steps described in Sec. IV. Steps a and b correspond to the cubic center and to the $Cr^{3+} - V_M$ center at the equilibrium geometry of the cubic center, respectively. In step c, only the F_{next} ion closest to the vacancy is relaxed.

Step	δ_t	δ_e
a	0	0
b	0.30	0.46
c	0.49	1.00
d	0.47	0.93
e	0.51	1.06

V. EXCITED STATES AND OPTICAL TRANSITIONS IN CUBIC AND $Cr^{3+} - V_M$ CENTERS

This section mainly looks into the effects of the Mg^{2+} vacancy on the crystal-field spectrum associated with the Cr^{3+} impurity using the highly accurate CASPT2 method.[45] In particular, we have explored the energies of selected states coming from the $t_{2g}^3(^2E_g), t_{2g}^2 e_g^1(^4T_{2g} + 1^4T_{1g})$, and $t_{2g}^1 e_g^2(2^4T_{1g})$ electronic configurations for both the cubic and the $Cr^{3+} - V_M$ centers. As in previous sections, we have performed these calculations in several steps to obtain some insight on the changes induced by the vacancy on electronic transitions. The main results are collected in Table VIII. In addition to values corresponding to the equilibrium geometry of the $Cr^{3+} - V_M$ center (step e), results obtained for step b where the $Cr^{3+} - V_M$ center is kept at the equilibrium geometry of the cubic center are also included in the table. It can first be noted that the present CASPT2 calculations for the cubic CrF_6^{3-} center are in reasonable agreement with available experimental data[11,24–26,32,33] and close to previous *ab initio* calculations by López-Moraza *et al.*[53] In particular, the present calculations indicate that the energy of $^4A_{2g} \to ^4T_{2g}$ and $^4A_{2g} \to ^2E_g$ transitions is rather close. Nevertheless, as Mortier *et al.* have shown in $KMgF_3 : Cr^{3+}$, a hydrostatic pressure of only 6 GPa changes the nature of the first excited

TABLE VIII. Representative values of energies (in cm^{-1}) derived by means of CASPT2 calculations for the d-d transitions of both the cubic and the $Cr^{3+} - V_M$ centers in $KMgF_3 : Cr^{3+}$. Aside from the values corresponding to the equilibrium geometry of the $Cr^{3+} - V_M$ center (step e), results obtained for step b where the $Cr^{3+} - V_M$ center is kept at the equilibrium geometry of the cubic center are also given. Experimental values for the cubic CrF_6^{3-} center (taken from Ref. 32) are also shown.

Transition		cubic CrF_6^{3-} (a)		$Cr^{3+}-V_M$	$Cr^{3+}-V_M$
Octahedral	Tetragonal	Calculated	Experimental	step b	step e
$^4A_{2g} \to ^4T_{2g}$	$^4B_1 \to ^4E$	15540	15200	15568	15069
	$^4B_1 \to ^4B_2$			15100	14745
$^4A_{2g} \to 1^4T_{1g}$	$^4B_1 \to ^4E$	23550	22570	22485	22630
	$^4B_1 \to ^4B_1$			25707	26970
$^4A_{2g} \to 2^4T_{1g}$	$^4B_1 \to ^4E$	38680	35090	37835	38586
	$^4B_1 \to ^4B_1$			37836	38929
$^4A_{2g} \to ^2E_g$	$^4B_1 \to ^2A_1$	17750	15360	17414	14366
	$^4B_1 \to ^2B_1$			17566	14675

state from $^4T_{2g}$ to ^2E_g.[11] The present calculations appear to overestimate a little the position of the ^2E_g state, which does not depend on 10 Dq.

Let us now focus on changes that take place on passing from the cubic to the $Cr^{3+} - V_M$ center. From results gathered in Table VIII it can be noted that the center of the gravity associated with $^4T_{2g} \rightarrow {}^4T_{2g}$, 1 $^4T_{1g}$, and 2 $^4T_{1g}$ transitions are found to be only slightly modified due to the addition of the Mg^{2+} vacancy and the associated electronic and structural relaxation. This conclusion thus concurs with available optical data. Along these lines, the splitting $\Delta_T = \Delta(^4E) - \Delta(^4B_2)$ induced by the Mg^{2+} vacancy on the $^4T_{2g}$ state is calculated to be only around 300 cm^{-1}, thus supporting that such a splitting is certainly smaller than the associated bandwidth, which is around 1500 cm^{-1} at low temperatures. As pointed out before, Vaills *et al.*, using available luminescence data, suggest that Δ_T for the $Cr^{3+} - V_M$ center in $KZnF_3 : Cr^{3+}$ would be $\sim 100 \text{ cm}^1$.[24]

It is worth noting that the value of Δ_T obtained by means of CASPT2 calculations (Table VIII) is smaller than the δ_t and δ_e splitting values collected in Table VII. If the $^4A_{2g}$ and $^4T_{2g}$ states in cubic symmetry are described only by a single Slater determinant, then Δ_T is given by[60]

$$\Delta_T = (3/4)(\delta_e - \delta_t). \tag{4}$$

Although this expression discards any configuration interaction in the description of states, it helps to understand why Δ_T can be smaller than the orbital splittings δ_t and δ_e.

Bearing in mind the results on the structural and electronic relaxations on the $Cr^{3+} - V_M$ center discussed in Secs. III and IV, it is surprising to see that the center of the gravity corresponding to the $^4A_{2g} \rightarrow {}^4T_{2g}$ transition is found to be shifted only by 4% with respect to the value for the pure cubic center. In a first view, it seems that such a center of gravity depends mainly on the *average* $Cr^{3+} - F^-$ distance in the CrF_6^{3-} unit perturbed by the Mg^{2+} vacancy. This standpoint can be somewhat related to what is found in the case of ruby. In the case of Cr^{3+}-doped Al_2O_3, the octahedron around the impurity is distorted as there are three ligands lying at 192 pm from the impurity while the rest are all placed at a distance equal to 202 pm.[61,62] Calculations of the center of gravity for the $^4A_{2g} \rightarrow {}^4T_{2g}$ transition carried out for real geometry give practically the same value as for a perfect octahedron where the ligands are all lying at the average distance 197 pm.[63]

With respect to transitions in the $Cr^{3+} - V_M$ center coming from $^4A_{2g} \rightarrow {}^2E_g$, the present results in Table VIII indicate that they are slightly underestimated as optical data seem to favor $^4B_2$ as a first excited state.[11,24,25]

VI. EPR PARAMETERS AND ELECTRONIC RELAXATION IN THE $Cr^{3+} - V_M$ CENTER

A. Anisotropy in the g tensor

The calculated values of the two transitions $^4B_1 \rightarrow {}^4B_2$ and $^4B_1 \rightarrow {}^4E$ [simply denoted as $\Delta(^4B_2)$ and $\Delta(^4E)$, respectively] support that such transitions are nearly coincident, and thus it is not easy to understand the experimental value $g_\perp - g_{||} = 3 \times 10^{-3}$ measured by Binois *et al.* for the $Cr^{3+} - V_M$ center in $KZnF_3$.[23] Indeed, if we use the expressions for $g_0 - g_{||}$

and $g_0 - g_\perp$ given in Eq. (1) and take $\xi^* = 165 \text{ cm}^{-1}$ and the figures $\Delta(^4B_2) = 14745 \text{ cm}^{-1}$ and $\Delta(^4E) = 15069 \text{ cm}^{-1}$ gathered in Table VIII, we find $g_\perp - g_{||} = 6 \times 10^{-4}$, which is thus *five times* smaller than the experimental value.

This puzzling situation can be overcome when we look in more detail into the origin of the g tensor. According to the C_{4v} symmetry of the $Cr^{3+} - V_M$ center, $g_0 - g_{||}$ arises from the admixture via spin-orbit coupling of the ground state with the $^4B_2$ state coming from $^4T_{2g}$ in O_h.[64] If no configuration interaction is considered, the transition from the ground to this $^4B_2$ state involves a $b_2(xy) \rightarrow b_1(x^2 - y^2)$ excitation where the two involved *orbitals* are lying in the plane *perpendicular* to the principal axis. Therefore, the admixture of the ground state with $^4B_2$ is determined by the $\langle \phi(xy)|h_{SO}|\phi(x^2 - y^2)\rangle$ matrix element, where the antibonding $|(i)$ orbitals ($i = xy, x^2 - y^2$) are briefly described by Eq. (3) and h_{SO} means the spin-orbit coupling operator for one electron. When $[N(i)]^2 > [\lambda(i)]^2$, then that matrix element can be approximated by

$$\begin{aligned} &\langle \phi(xy)|h_{SO}|\phi(x^2 - y^2)\rangle \\ &\cong N(xy)N(x^2 - y^2)\langle d(xy)|h_{SO}|d(x^2 - y^2)\rangle. \end{aligned} \tag{5}$$

Therefore, taking into account Stone's expression,[65] $g_0 - g_{||}$ can be written as

$$g_0 - g_{||} = \frac{8}{3}k_{||}\frac{\xi}{\Delta(^4B_2)}. \tag{6}$$

Here $\xi = 270 \text{ cm}^{-1}$ denotes the spin-orbit coefficient of a *free* chromium ion and $k_{||} = [N(xy)]^2[N(x^2 - y^2)]^2$ conveys the reduction due to covalency. Similarly, $g_\perp - g_0$ can be viewed to arise from an $yz \rightarrow y^2 - z^2$ excitation and thus $g_0 - g_\perp$ is given by

$$g_0 - g_\perp = \frac{8}{3}k_\perp\frac{\xi}{\Delta(^4E)}, \tag{7}$$

where $k_\perp = [N(yz)]^2\{\frac{3}{4}[N(3z^2 - r^2)]^2 + \frac{1}{4}[N(x^2 - y^2)]^2\}$. Therefore, according to Eqs. (6) and (7), the *reduction* factors $k_{||}$ and $k_\perp$ are not necessarily equal under a C_{4v} symmetry. Furthermore, from the present study, $k_{||}$ is expected to be higher than $k_\perp$ because the presence of the vacancy decreases the charge on chromium more on orbitals with an *axial* character (like $3z^2 - r^2$ or xz,yz) than for those lying in the plane *perpendicular* to the C_{4v} axis. Quantitatively, putting in Eqs. (6) and (7) the values of $[N(i)]^2$ quantities gathered in Table V, we obtain $k_{||} = 0.72$ and $k_\perp = 0.62$. It should be stressed now that this difference between the two reduction factors, although small, induces a huge increase of the $g_\perp - g_{||}$ quantity as it becomes equal to 5×10^{-3} and thus an order of magnitude higher than the value derived through Eq. (1). Therefore, this analysis shows that the *different* electronic relaxation induced by the vacancy upon the five antibonding orbitals plays a key role for understanding the anisotropy in the g tensor measured experimentally.

B. Superhyperfine tensor

According to the results embodied in Secs. IV and VI, experimental quantities reflecting in a *direct* way the *local* electronic density are expected to be particularly sensitive

to the presence of a nearby vacancy. This condition is well fulfilled by the shf tensor of the six involved ligands.

For the sake of clarity, let us first consider the octahedral CrF_6^{3-} center where the diagonal shf tensor of a given ligand is described by two components, $A_{||}$ and $A_{\perp}$. The first (second) component describes the interaction between the electronic spin, $\mathbf{S}$, and the spin, $\mathbf{I}$, of an F nucleus when $\mathbf{S}$ is parallel (perpendicular) to the corresponding Cr-F axis. There are three main contributions to the shf tensor of a CrF_6^{3-} center with a $^4A_{2g}(t_{2g}^3)$ ground state,[58]

$$A_{||} = A_{CP} + 2(A_D - A_{\pi}), \quad A_{\perp} = A_{CP} - (A_D - A_{\pi}), \quad (8)$$

where

$$A_D \cong \frac{2\beta g_N \beta_N}{R^3}, \quad A_{\pi} = f_{\pi} \frac{A_p^0}{3}. \quad (9)$$

In Eqs. (8) and (9), A_{π} originates from the presence of unpaired spin density on a ligand π orbital due to bonding while A_D reflects the classical magnetic-dipole interaction between unpaired electrons, lying mostly on chromium, and the fluorine nucleus. A_{CP} denotes the core polarization contribution while the value of A_p^0 for fluorine is 1320 MHz.

From the experimental values $A_{||} = -26.5$ MHz and $A_{\perp} = 8.5$ MHz reported for the CrF_6^{3-} center in $KZnF_3$,[23] we obtain $A_{CP} = -3$ MHz and $A_{\pi} = 22.5$ MHz, taking $A_D = 10.8$ MHz. Very close values have been measured for the same center in $KMgF_3$.[58,66] This analysis thus reveals that A_{π} is the *dominant* contribution to the shf tensor for the cubic center. Moreover, from Eq. (9) and $A_{\pi} = 22.5$ MHz we obtain $f_{\pi} = 5\%$. A close figure has been derived from the present calculations as shown in Table VI.

With regard to the $Cr^{3+} - V_M$ center in $KZnF_3$, partial experimental information on the shf interaction has been reported.[23] In particular, the $A_{||}$ component corresponding to the two ligands lying along the C_4 axis has been measured. For one such ligand, it is found $A_{||} = -23.1$ MHz, while for the other $A_{||} = -33.6$ MHz. Therefore, $|A_{||}|$ is 46% higher for the last ligand than for the former. As for the cubic CrF_6^{3-} center, $A_{||}$ is dominated by the A_{π} contribution reflecting directly f_{π}, and the value $A_{||} = -33.6$ MHz should correspond to the F_{next} ligand according to the results on f_{π} calculated for the $Cr^{3+} - V_M$ center (Table VI). This conclusion is reinforced by the electron nuclear double resonance (ENDOR) results carried out on $K_2MgF_4 : Cr^{3+}$ (Ref. 29) where the trigonal center involving a close K^+ vacancy has been investigated in detail. In this case, it has been measured $A_{||} = -30.4$ MHz and $A_{\perp} = 15.3$ MHz for the three closest ligands, while $A_{||} = -26.4$ MHz and $A_{\perp} = 10.0$ MHz for the three farthest ones. Therefore, the results reported by Binois *et al.*[23] are consistent with a significant increase of f_{π} on passing from the farthest ligand to the closest one. Although this *trend* is reproduced by the present calculations (Table VI), a further analysis would require us to measure the experimental $A_{\perp}$ quantity for both F_{far} and F_{next} ligands and thus determine the corresponding values of A_{CP} and A_{π} contributions.

VII. FINAL REMARKS

The present calculations on both the cubic and $Cr^{3+} - V_M$ centers formed in $KMgF_3 : Cr^{3+}$ shed light on the structural and electronic relaxations induced by the vacancy and its influence upon optical and EPR parameters. Aside from a 7% reduction on the $Cr^{3+} - F_{next}$ distance, the total charge on this ligand decreases significantly ($0.2e$) on passing from the cubic to the $Cr^{3+} - V_M$ center, even freezing the geometry of the former center. That charge is transferred to the F_{far} ligand and also to the four equatorial ligands. Accordingly, f_{π} is found to be higher for F_{next} than for the F_{far} ligand, thus supporting a higher $|A_{||}|$ value for the former than for the latter ligand.

In spite of the structural and electronic relaxation due to the vacancy, the present CASPT2 results support that the center of the gravity for the $^4A_{2g} \rightarrow ^4T_{2g}$ transition of the $Cr^{3+} - V_M$ center is little affected by the vacancy, whereas the Δ_T splitting is certainly small when compared to the corresponding bandwidth. Therefore, properties that exhibit a *global* character seem to be much less influenced by the electronic relaxation than those depending mainly on the electronic density *at a given point* of the $Cr^{3+} - V_M$ center. This is the case of hyperfine interactions with the involved nuclei, which, as discussed in this work, can be significantly altered by the presence of the vacancy. Along these lines, the *slightly* smaller charge on chromium for axial orbitals [like $a_1(3z^2 - r^2)$] than for those [like $b_1(x^2 - y^2)$] lying in a perpendicular plane to the C_4 axis explains why the anisotropy in the g tensor is well observed experimentally, although the calculated Δ_T value is only 300 cm^{-1}. Accordingly, EPR and optical data for the $Cr^{3+} - V_M$ center can finally be conciliated.

The present results on the $Cr^{3+} - V_M$ *model* center can be of help in gaining a better insight into the role played by vacancies in the electronic properties of insulating materials. In particular, this study stresses that a *consistent* explanation of *all* electronic properties influenced by a close vacancy cannot be reached ignoring that ions are not rigid spheres. Consequently, the phenomenological potentials used for studying *big* systems involving vacancies should incorporate in some way the effects of electronic relaxation well proved in this work.

From the present study on complex impurity-vacancy centers, the variations of the electronic charge due to the presence of a close vacancy are expected to be especially significant for ligands lying along the axis joining the impurity and the vacancy. This standpoint is verified in the case of the $Rh^{2+} - V_M$ center formed in NaCl when compared to the pure $RhCl_6^{4-}$ species, which exhibits a static Jahn-Teller effect.[12,67] Indeed, while the two components of the hyperfine tensor for $RhCl_6^{4-}$ are found to be null, the addition of a close Na^+ vacancy in a $\langle 001 \rangle$ direction gives rise to a measurable hyperfine interaction for the $Rh^{2+} - V_M$ center.[67,68] Nevertheless, a distortion in this center driven by the pseudo-Jahn-Teller effect causes the unpaired electron to be placed in an orbital lying perpendicular to the $Rh^{2+} - V_M$ axis. Accordingly, the biggest superhyperfine interaction takes place with two ligands that are not along the $Rh^{2+} - V_M$ axis and are thus less influenced by the presence of the Na^+ vacancy.

As a main conclusion, this analysis shows that experimental techniques that are able to probe the local density are especially sensitive to the presence of a point defect like a vacancy coupled to the impurity. Bearing in mind that the biggest effects appear along the C_4 axis, it is interesting to study impurities like Fe^{3+} or Mn^{2+} with one unpaired electron lying in that axis and displaying a σ character. In principle, important changes on the f_σ and f_s quantities of axial ligands are expected. To our knowledge, no clear experimental information on the superhyperfine tensor for the $Fe^{3+} - V_M$ center in fluorides has been reported, but there are good EPR data on the FeF_5O^{4-} centers formed in KMF_3 fluorides (M = Mg, Zn) demonstrating a significant reduction of f_s in the axial ligand due to the presence of O^{2-}.[5,21,69,70] Preliminary calculations on the $Fe^{3+} - V_M$ center in $KMgF_3$ show the existence of an important increase of f_σ induced by the vacancy in the closest ligand. Further work along these lines is now underway.

[1] J. Friedel, *Dislocations* (Pergamon, Oxford, 1964), Chap. 4.

[2] A. B. Lidiard, in *Theory of Imperfect Crystalline Solids*, edited by International Centre for Theoretical Physics in Trieste (International Atomic Energy Agency, Vienna, 1971).

[3] J. B. Goodenough, Nature (London) **404**, 821 (2000).

[4] X. Yang, H. Li, J. Xu, Y. Cheng, L. Su and Q. Tang, J. Am. Ceram. Soc. **91**, 3098 (2008).

[5] M. Moreno, M. T. Barriuso, J. A. Aramburu, P. Garcia-Fernandez, and J.M. Garcia-Lastra, J. Phys.: Condens. Matter **18**, R315 (2006).

[6] G. D. Watkins, Phys. Rev. **113**, 79 (1959).

[7] J. E. Wertz and P. V. Auzins, J. Phys. Chem. Solids **28**, 1557 (1967).

[8] R. K. Jeck and J. J. Krebs, Phys. Rev. B **5**, 1677 (1972).

[9] M. Vanhaelst, P. Matthys, and E. Boesman, Phys. Status Solidi B **78**, 553 (1976).

[10] E. Siegel and K. A. Muller, Phys. Rev. B **19**, 109 (1979).

[11] M. Mortier, Q. Wang, J. Y. Buzaré, M. Rousseau, and B. Piriou, Phys. Rev. B **56**, 3022 (1997).

[12] H. Vrielinck, F. Callens, and P. Matthys, Phys. Rev. B **64**, 214105 (2001).

[13] F. La Mattina, J. G. Bednorz, S. F. Alvarado, A. Shengelaya, K. A. Muller, and H. Keller, Phys. Rev. B **80**, 075122 (2009).

[14] S. Pöykkö and D. J. Chadi, Phys. Rev. Lett. **83**, 1231 (1999).

[15] P. Erhart, R.-A. Eichel, P. Träskelin, and K. Albe, Phys. Rev. B **76**, 174116 (2007).

[16] Y. Tokura, Rep. Prog. Phys. **69**, 797 (2006).

[17] C. M. Handley, G. I. Hawe, D. B. Kell, and P. L. A. Popelier, Phys. Chem. Chem. Phys. **11**, 6365 (2009).

[18] D. J. Newman and B. Ng, Rep. Prog. Phys. **52**, 699 (1989).

[19] P. Gnutek, Z. Y. Yang, and C. Rudowicz, J. Phys.: Condens. Matter **21**, 455402 (2009).

[20] H. Meštrić, R.-A. Eichel, T. Kloss, K.-P. Dinse, S. Laubach, S. Laubach, P. C. Schmidt, K. A. Schönau, M. Knapp, and H. Ehrenberg, Phys. Rev. B **71**, 134109 (2005).

[21] J. M. Garcia-Lastra, M. T. Barriuso, J. A. Aramburu, and M. Moreno, Appl. Magn. Reson. **34**, 149 (2008).

[22] J. L. Patel, J. J. Davies, B. C. Cavenett, H. Takeuchi, and H. Horai, J. Phys. C **9**, 129 (1976).

[23] M. Binois, A. Leble, J. J. Rousseau, and J. C. Fayet, J. Phys. (Paris) Colloq. **34**, C9-285 (1973).

[24] Y. Vaills, J. Y. Buzaré, and M. Rousseau, J. Phys.: Condens. Matter **2**, 3997 (1990).

[25] D. R. Lee, T. P. J. Han, and B. Henderson, Appl. Phys. A **59**, 365 (1994).

[26] B. Villacampa, J. C. González, R. Alcalá, and P. J. Alonso, J. Phys.: Condens. Matter **3**, 8281 (1991).

[27] B. Henderson and R. H. Bartram, in *Crystal Field Engineering of Solid State Laser Materials* (Cambridge University Press, Cambridge, 2000).

[28] C. E. Webb and J. D. C. Jones, *Handbook of Laser Technology and Applications* (Institute of Physics, London, 2003).

[29] H. Takeuchi, M. Arakawa, H. Aoki, T. Yosida, and K. Horai, J. Phys. Soc. Jpn. **51**, 3166 (1982).

[30] M. Arakawa, H. Ebisu, and H. Takeuchi, J. Phys. Soc. Jpn. **55**, 2853 (1986).

[31] J. J. Davies and K. Horai, J. Phys. C **4**, 682 (1971).

[32] N. S. Altshuler and L. Larionov, Opt. Spectrosc. **66**, 61 (1989).

[33] O. Pilla, E. Galvanetto, M. Montagna, and G. Viliani, Phys. Rev. B **38**, 3477 (1988).

[34] H. Takeuchi and M. Arakawa, J. Phys. Soc. Jpn. **53**, 376 (1984).

[35] G. F. Imbusch, A. L. Schawlow, A. D. May and S. Sugano, Phys. Rev. **140**, A830 (1965).

[36] A. Abragam and B. Bleaney, *Electron Paramagnetic Resonance of Transition Ions* (Clarendon, Oxford, 1970).

[37] J. M. García-Lastra, M. T. Barriuso, J. A. Aramburu, and M. Moreno, J. Phys.: Condens. Matter **22**, 155502 (2010).

[38] G. te Velde, F. M. Bickelhaupt, E. J. Baerends, C. F. Guerra, S. J. A. Van Gisbergen, J. G. Snijders, and T. Ziegler, J. Comput. Chem. **22**, 931 (2001).

[39] S. H. Vosko, L. Wild and M. Nusair, Can. J. Phys. **58**, 1200 (1980).

[40] A. D. Becke, Phys. Rev. A **38**, 3098 (1988).

[41] J. P. Perdew, Phys. Rev. B **33**, 8822 (1986).

[42] J. P. Perdew, in *Electronic Structure of Solids*, edited by P. Ziesche and H. Eschrig (Akademie Verlag, Berlin, 1991), p. 11.

[43] M. Ernzerhof and G. Scuseria, J. Chem. Phys. **110**, 5029 (1999).

[44] C. Adamo and V. Barone, J. Chem. Phys. **110**, 6158 (1999).

[45] K. Andersson, P. A. Malmqvist, and B. O. Roos, J. Chem. Phys. **96**, 1218 (1992).

[46] G. Pacchioni, F. Frigoli, D. Ricci, and J. A. Weil, Phys. Rev. B **63**, 054102 (2000).

[47] C. Sousa, C. de Graaf, F. Illas, M. T. Barriuso, J. A. Aramburu, and M. Moreno, Phys. Rev. B **62**, 13366 (2000).

[48] L. Hozoi, C. Presura, C. de Graaf, and R. Broer, Phys. Rev. B **67**, 035117 (2003).

[49] *MOLCAS 7.0*, K. Andersson, F. Aquilante, M. Barysz, E. Bednarz, A. Bernhardsson, M. R. A. Blomberg, Y. Carissan, D. L. Cooper,

M. Cossi, A. Devarajan, L. De Vico, N. Ferré, M. P. Fülscher, A. Gaenko, L. Gagliardi, G. Ghigo, C. de Graaf, B. A. Hess, D. Hagberg, A. Holt, G. Karlström, J. W. Krogh, R. Lindh, P.-Å. Malmqvist, T. Nakajima, P. Neogrády, J. Olsen, T. B. Pedersen, J. Raab, M. Reiher, B. O. Roos, U. Ryde, B. Schimmelpfennig, M. Schütz, L. Seijo, L. Serrano-Andrés, P. E. M. Siegbahn, J. Stålring, T. Thorsteinsson, V. Veryazov, P.-O. Widmark, and A. Wolf, Lund University, Sweden (2007).

[50] L. Seijo and Z. Barandiarán, in *Computational Chemistry: Reviews of Current Trends*, edited by J. Leszczynski (World Scientific, Singapore, 1999).

[51] B. O. Roos, in *New Challenges in Computational Quantum Chemistry*, edited by R. Broer, P. J. C. Aerts, and P. S. Bagus (Groningen, The Netherlands, 1994), p. 12.

[52] R. W. G. Wyckoff, *Crystal Structures* (Krieger, Florida, 1986), Vol. II.

[53] S. López-Moraza, L. Seijo, and Z. Barandiarán, Int. J. Quantum Chem. **77**, 961 (2000).

[54] M. Moreno, J. M. García-Lastra, M. T. Barriuso, and J. A. Aramburu, Theor. Chem. Account **118**, 665 (2007).

[55] P. García-Fernández, I. B. Bersuker, J. A. Aramburu, M. T. Barriuso, and M. Moreno, Phys. Rev. B **71**, 184117 (2005).

[56] P. García-Fernández, C. Sousa, J. A. Aramburu, M. T. Barriuso, and M. Moreno, Phys. Rev. B **72**, 155107 (2005).

[57] A.-J. Mao and X.-Y. Kuang, J. Phys. Chem. A **112**, 7285 (2008).

[58] B. C. Tofield, J. Phys. (Paris) Colloq. **37**, C6-539 (1976).

[59] A. Trueba, J. M. García-Lastra, M. T. Barriuso, J. A. Aramburu, and M. Moreno, Phys. Rev. B **78**, 075108 (2008).

[60] M. T. Barriuso, J. A. Aramburu, and M. Moreno, Phys. Status Solidi B **196**, 193 (1996).

[61] E. Gaudry, A. Kiratisin, P. Sainctavit, C. Brouder, F. Mauri, A. Ramos, A. Rogalev, and J. Goulon, Phys. Rev. B **67**, 094108 (2003).

[62] E. Gaudry, D. Cabaret, C. Brouder, I. Letard, A. Rogalev, F. Wilhlem, N. Jaouen, and P. Sainctavit, Phys. Rev. B **76**, 094110 (2007).

[63] J. M. García-Lastra, J. A. Aramburu, M. T. Barriuso, and M. Moreno, Phys. Rev. B **74**, 115118 (2006).

[64] R. Lacroix and G. Emch, Helv. Phys. Acta **35**, 592 (1962).

[65] A. J. Stone, Proc. R. Soc. London, Ser. A **271**, 424 (1963).

[66] J. J. Davies and H. Horai, J. Phys. C **4**, 671 (1971).

[67] H. Vercammen, D. Schoemaker, H. Käss, E. Goovaerts, A. Bouwen, H. Vrielink, and F. Callens, J. Appl. Phys. **84**, 428 (1998).

[68] M. T. Barriuso, J. A. Aramburu, and M. Moreno, J. Phys.: Condens. Matter **14**, 6521 (2002).

[69] D. C. Stjern and R. C. DuVarney, Phys. Rev. **10**, 1044 (1974).

[70] J. Y. Buzaré and J. C. Fayet, Solid State Commun. **21**, 1097 (1977).